New Observations of Precipitation Initiation in Warm Cumulus Clouds

JENNIFER D. SMALL AND PATRICK Y. CHUANG

Cloud and Aerosol Laboratory, University of California, Santa Cruz, Santa Cruz, California

(Manuscript received 27 August 2007, in final form 1 February 2008)

ABSTRACT

The mechanism responsible for formation of rain in warm clouds has been debated for over six decades. Here, the authors analyze new measurements of shallow cumulus made with a phase Doppler interferometer during the Rain in Cumulus over the Ocean (RICO) experiment. These observations show that drops sufficiently large (>55-μm diameter) to initiate precipitation (termed collision–coalescence initiators or CCIs) are found preferentially at cloud top, tend to cluster with each other, and are found in environments that are thermodynamically, dynamically, and microphysically distinct from those of smaller drops. The CCI environments exhibit cloud spectra that are shifted to larger sizes, with enhanced broadening toward larger drop sizes. Increased entrainment is also associated with CCIs, suggesting that it is an important process in CCI production. A simple model combining inhomogeneous mixing and condensation is inadequate to explain these observations. It is hypothesized that CCIs are produced in cloud-top regions where turbulence generated by entrainment mixing locally enhances collision–coalescence rates.

1. Introduction

The initiation of precipitation in warm clouds has yet to be adequately explained (Illingworth 1988; Beard and Ochs 1993; Laird et al. 2000). Warm rain formation requires that over ~10–30 min (Beard and Ochs 1993; Johnson 1993), cloud drops formed by condensation (~10–20 μm in diameter) must grow to become raindrops (Baker and Latham 1979; Rogers and Yau 1989) through collision–coalescence. It has been shown that if a few drops with diameters 55 μm and greater—here termed collision–coalescence initiators (CCIs)—are present, then precipitation can form within the observed time scales (Johnson 1993). However, the origin of CCIs has not been adequately explained or validated by appropriate in-cloud measurements, in part because of instrument size range and accuracy limitations as well as problems with sampling statistics (Baumgardner and Spowart 1990; Cooper 1988; Glantz et al. 2003).

Several mechanisms have been proposed to explain warm rain formation in cumuli, including the existence of ultragiant aerosols (UGAs; Johnson 1982; Lasher-Trapp et al. 2002; Blyth et al. 2003), inhomogeneous (Latham and Reed 1977; Lasher-Trapp et al. 2005) and homogeneous entrainment mixing (Telford et al. 1984), and small-scale turbulence (Jonas 1996; Shaw, 2003; Tisler et al. 2005).

The simplest mechanism invoked to explain the formation of CCIs is the presence of UGAs (dry diameter >20 μm) in the aerosol population (Johnson 1976). Although present in small concentrations that vary by several orders of magnitude, from 10^{-2} cm^{-3} for smaller sizes and 10^{-8} cm^{-3} for the larger sizes (Noll and Pilat 1971; Meszaros and Vissy 1974; Johnson 1976), UGAs may serve an important role in the initiation of precipitation. In this case, coalescence is thought to begin after larger drops formed on UGAs reach a size such that their gravitational settling velocity is significantly different than that of typical cloud drops (Lasher-Trapp et al. 2001). This allows precipitation initiation to begin faster than predicted if UGAs were not present and without needing to invoke mixing and entrainment hypotheses.

A more complex and less understood mechanism that may play a role in the warm rain process is the entrainment of dry air at cloud–air boundaries. There is strong evidence that entrainment occurs at all levels within cumulus clouds, influencing the evolution of drop size distributions during cloud development. The cloud top, especially the ascending tops of growing clouds such as trade wind cumuli, has been identified as

Corresponding author address: Patrick Y. Chuang, Earth and Planetary Sciences Department, University of California, Santa Cruz, 1156 High Street, Santa Cruz, CA 95064.
E-mail: pchuang@es.ucsc.edu

DOI: 10.1175/2008JAS2600.1

one of the key locations for entrainment and likely resulting in the development of penetrative downdrafts (Squires 1958; Paluch 1979). Two end-member mixing models, homogeneous and inhomogeneous, are typically invoked to explain the effect of entrainment on drop size distributions and total cloud drop concentration.

In the "classical" homogeneous mixing model (Warner 1969a,b, 1970, 1973), the parcel of cloudy air is perfectly mixed across its whole breadth as soon as dry environmental air is entrained. Telford et al. (1984) describe this process as an extreme case in which every droplet is associated after mixing with a tiny volume of dry air in proportion to the drop-free space in its immediate vicinity; thus, each drop experiences the same humidity decrease. Each drop then partly evaporates to saturate the tiny volume of dry air (Telford et al. 1984). Baker et al. (1980) provide a similar definition such that for a mixing process to be considered homogeneous, all droplets at a given level in the cloud are, at any time, exposed to identical conditions of undersaturation, resulting in a shift in the drop size distribution to smaller sizes without decreasing the total number of drops.

An alternative to the classical mixing model is that of Baker et al. (1980), who define inhomogeneous mixing as the intermingling of cloudy and environmental air as a highly inhomogeneous process in which the droplets immediately adjacent to the infiltrating parcels of undersaturated air are drastically affected, whereas those that are more remote are less affected or even completely unaffected. In the extreme, this model leads to the complete evaporation of some drops of each size. The resulting size distribution resembles the original in shape but with a decrease in total number of drops within each size class. This is thought to provide appropriate conditions for the growth of CCIs within observed time scales (see section 5).

Similar to entrainment but on a smaller (mm to cm) scale, many researchers support the theory that turbulence should result in the broadening of the droplet spectrum (Pinsky and Khain 1996; Khain and Pinsky 1997; Shaw et al. 1998; Pinsky et al. 1999). The spectrum may be broadened as a result of enhanced collision/coalescence of droplets (Jonas 1996; Vohl et al. 1999; Wang et al. (2006), preferential concentration of droplets (Shaw et al. 1998), and turbulent fluctuations in supersaturation (Shaw et al. 1998; Vaillancourt and Yau 2000; Brenguier and Chaumat 2001; Shaw 2003).

A longstanding goal of cloud physics research has been to evaluate the plausibility of the aforementioned mechanisms via accurate observations of CCIs in cloud in conjunction with in situ meteorological and aerosol measurements. We note that these mechanisms are not necessarily mutually exclusive, and in principle combinations of them may be required to properly explain warm rain initiation. In the following sections, we attempt to evaluate these mechanisms to understand the role they play in the initiation of precipitation. Specifically, section 2 briefly describes the instrumentation, section 3 describes the meteorological conditions and flight plan used in the study, section 4 presents and discusses our observations made with new instrumentation using a novel method of data analysis, and section 5 utilizes a simple mixing and condensation model to attempt to explain and reproduce observed characteristics of the drop spectrum.

2. Instrumentation

The present study describes observations of CCIs in small trade wind cumuli made during the Rain in Cumulus over the Ocean (RICO) campaign (Rauber et al. 2007) and examines which of these mechanisms are consistent with the observations. Observations were made with a phase Doppler interferometer (PDI; Sankar et al. 1994; Bachalo and Sankar 1998; Strakey et al. 2000; Widmann et al. 2001; Chuang et al. 2008) on the National Center for Atmospheric Research C130 aircraft during RICO in January 2005 and obtained drop size distributions for the size range 4–200 μm (all sizes are reported herein as the diameter D_p). The PDI differs from more conventional light scattering intensity-based optical cloud probes in that measurements rely on a view volume where intersecting lasers create an interference pattern. The phase difference between two recorded signals is a measure of drop size, provided the drops are spherical with a known refractive index. Comparisons with a traditional forward scattering spectrometer probe (FSSP-100) during the RICO experiment show that there are systematic differences in the measured size distribution mean (PDI larger then FSSP by 5 μm) and breadth (FSSP broader by 20%–50%), although these biases are not so large that it would greatly impact the results of this paper. One important advantage of the PDI relative to FSSP for the observations described here is that coincidence of two smaller cloud drops in the view volume will not be registered as a single, larger drop—a problem that leads to difficulties in interpreting FSSP data at larger drop sizes. The RICO project was the first deployment of the PDI and the cross-sectional sampling area was unusually small, $\sim$0.025 mm^2; under current operating conditions the sampling area is about a factor of 10 higher. This resulted in an undersampling of drops as compared to the FSSP during RICO. For more detailed information regarding uncertainties in derived quantities, instrument

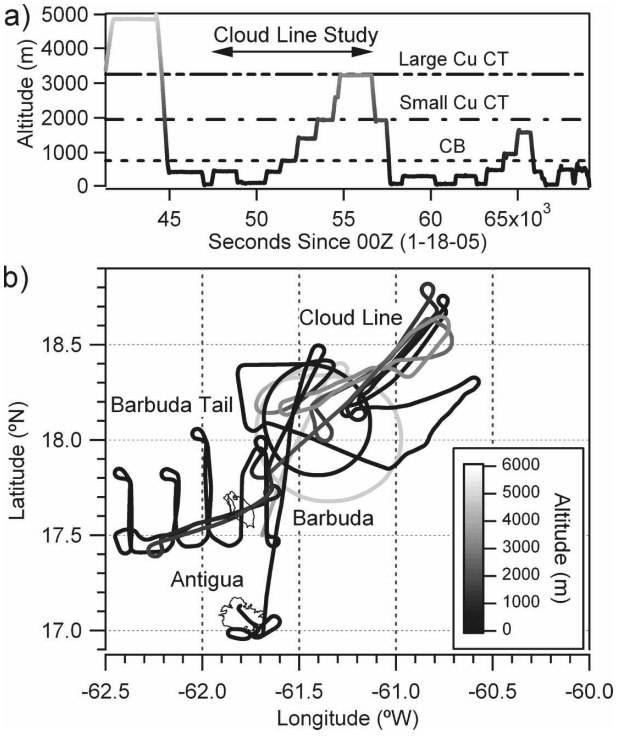

FIG. 1. Altitude and flight path for Research Flight 16. (a) Altitude profile with cloud line study noted (between 1310 and 1540 UTC). Broken lines mark cloud base (dotted), small cumulus cloud tops (dotted–dashed) and tops of larger cumulus (triple dotted–dashed). (b) Flight track for RF16 with line shading showing altitude.

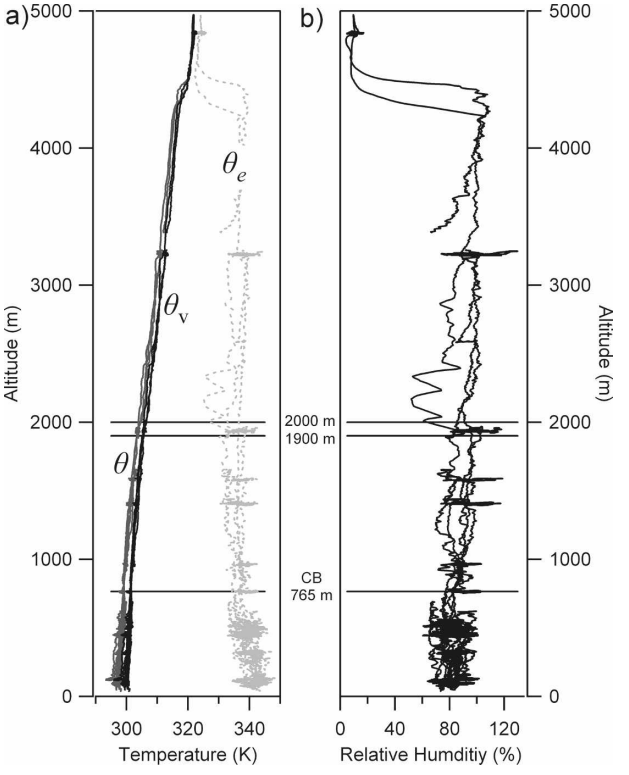

FIG. 2. Environmental sounding on RF16 for (a) θ, θ_e, and θ_v (dark gray solid line, black solid line, and light gray dotted line, respectively) and (b) relative humidity as a function of altitude.

specifications, and performance, see Chuang et al. (2008) and Bachalo and Sankar (1998). Other measurements in this analysis include a FSSP-100 and a 2D Cloud Probe (2DC), both manufactured by Particle Measuring Systems, Inc., and a King Liquid Water Probe.

3. Meteorological conditions and flight plan

The cumulus sampled during the NCAR-C130 flight Research Flight 16 (RF16, 18 January 2005) were part of a convective line extending northeast off the coast of Barbuda. Similar precipitating convective lines were sampled during two other January research flights (RF11 and RF15). The vertical thickness of the small cumuli (the focus of this study; see next section) was ~1200 m, whereas that for larger cumuli was ~2500 m. The data for this study were collected from one segment of RF16 at 1900–2000 m between 1451 and 1506 UTC and from the Barbuda island tail between 1547 and 1557 UTC (see Fig. 1 for flight track and altitude profile). Precipitation was observed below cloud and during cloud penetrations through midlevels of larger clouds. The vertical environmental soundings of relative humidity and thermodynamic variables are shown in Fig. 2 with the cloud-base altitude and lines for the altitude range of the observations.

4. Observations

Drop size measurements were made at all in-cloud sampling altitudes with greater frequency of occurrence of CCIs at higher altitudes (Figs. 3a,b). Two primary regions of CCIs are identified, corresponding to sampling altitudes of 1900–2000 m (denoted CT in Fig. 3), at the tops of small cumuli and midlevels of large cumuli, and 3200–3300 m, at the tops of large precipitating cumuli. Hereafter, we focus only on observations in the tops of nonprecipitating small cumuli. Precipitating clouds were eliminated if the 2DC measured a concentration of more than 1 L^{-1} for drops with $D_p > 0.5$ mm, a typical lower size bound for small rain drops. Measurements made at midlevels of large cumuli were also usually eliminated using this threshold because they were typically precipitating, but this was further confirmed by flight notes and forward-facing video to en-

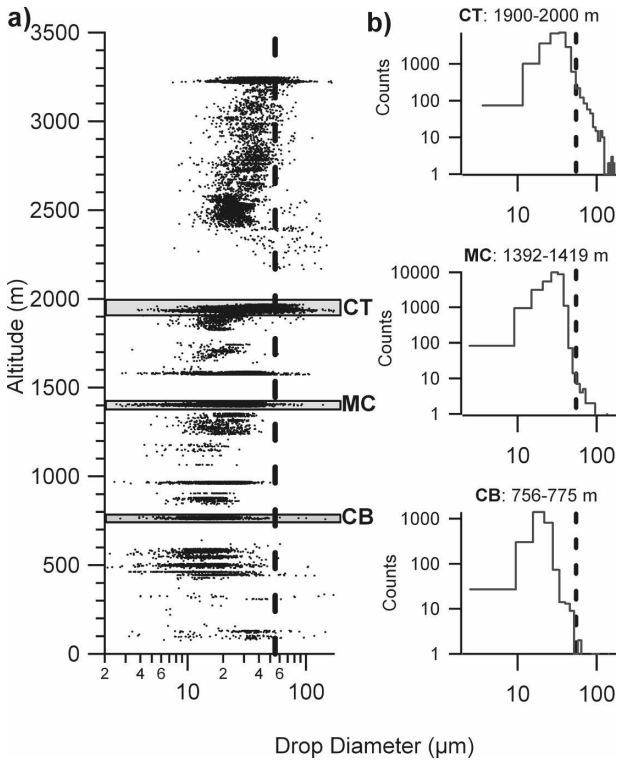

FIG. 3. (a) Altitudes for PDI drop diameter observations. Black dots represent individual droplet observations; gray boxes outline flight levels for cloud base (CB), a midcloud level (MC), and cloud top (CT) for the shallow cumulus. (b) Frequency size distributions for the three example levels CB, MC, and CT. For both (a) and (b), thick dashed lines denote a drop diameter of 55 μm.

sure that our observations include only the tops of small cumuli.

For each drop observed by the PDI, its size and arrival time are recorded and then filtered based on the criteria described above. Using PDI drop arrival times, we then determine environmental characteristics in a 1-s time envelope surrounding each observed drop, which is termed the "central drop" for that envelope (conceptually illustrated in Fig. 4). The envelope is centered on the arrival time t of the central drop (i.e., the envelope ranges from $t - 0.5$ s to $t + 0.5$ s). Note that any given envelope can overlap with other envelopes and almost always does. For each envelope, a number of characteristics are determined: the shape of the cloud drop size distribution measured by PDI; the mean and standard deviation (σ) of PDI cloud drop number concentration (N_d); the fraction of drops considered to be CCIs (N_{CCI}/N_d)—that is, the fraction of drops with $D_p > 55$ μm; the mean and σ of vertical velocity (w); the mean and σ of King Probe liquid water content (LWC); and the mean and σ of potential temperature (θ), equivalent potential temperature (θ_e), and virtual potential temperature (θ_v). This quantifies the cloud dynamic, thermodynamic, and microphysical context for each observed drop. The true airspeed of the C130 for RF16 during the sampling period was 119 $\pm$ 2 m s^{-1}. Thus, each 1-s window represents a ~119-m segment. Analyses utilizing time envelopes of 0.5 and 0.25 s (rather than 1 s) were also completed. These results are quantitatively very similar and thus not shown.

We describe here a few caveats regarding the above parameters. Mean LWC and w values reported in this study are low, similar to observations in stratiform clouds. This is expected because only cloud-top samples, where LWC is reduced by entrainment and w is typically close to zero or slightly negative, are included in the analysis. Also, PDI cloud drop number concentrations were determined by scaling to match FSSP N_d in the overlap size range. This was necessary because the data did not permit the normal and independent determination of PDI view volume (Chuang et al. 2008) We choose to use the King probe liquid water content rather than the PDI because the small sample volume does not allow us to generate reasonable 25-Hz (or even 1 Hz) LWC from the PDI.

Because the PDI measures drops individually and 1-s drop environments are independently calculated for each drop, it is possible to investigate the relationship of the size of the central drop to its environmental conditions (i.e., the characteristics in the surrounding 1-s envelope). To do so, we sort all the observations by the central drop size. We use this novel envelope technique rather than a traditional fixed-frequency analysis (i.e., at 1 or 25 Hz) to specifically investigate the environment surrounding individual drops regardless of spatial location. A fixed-frequency analysis is not appropriate for our purposes because it prevents overlapping samples. A strength of this analysis is that simultaneous intercomparisons between all parameters for the environment surrounding an individual drop are possible. This makes this analysis complementary to traditional, fixed-frequency analysis methods. Because the spacing of CCIs is also of interest (note that this analysis prevents direct assessment of drop spacing due to overlapping samples), a supplemental fixed-frequency analysis was also conducted and is discussed later.

Figures 5–7 show the envelope properties after sorting by the central drop size for drops measured at the sampling altitude of 1900–2000 m after filtering. Figure 5 shows drop size distributions, presented in percentiles where D_n is the droplet diameter such that n% of the droplets are smaller than D_n (after Brenguier and Chaumat 2001). Here we highlight the tenth (D_{10}), fiftieth or median (D_{50}), and ninetieth (D_{90}) percentiles to indicate the shape and width of the drop spectra. Of the

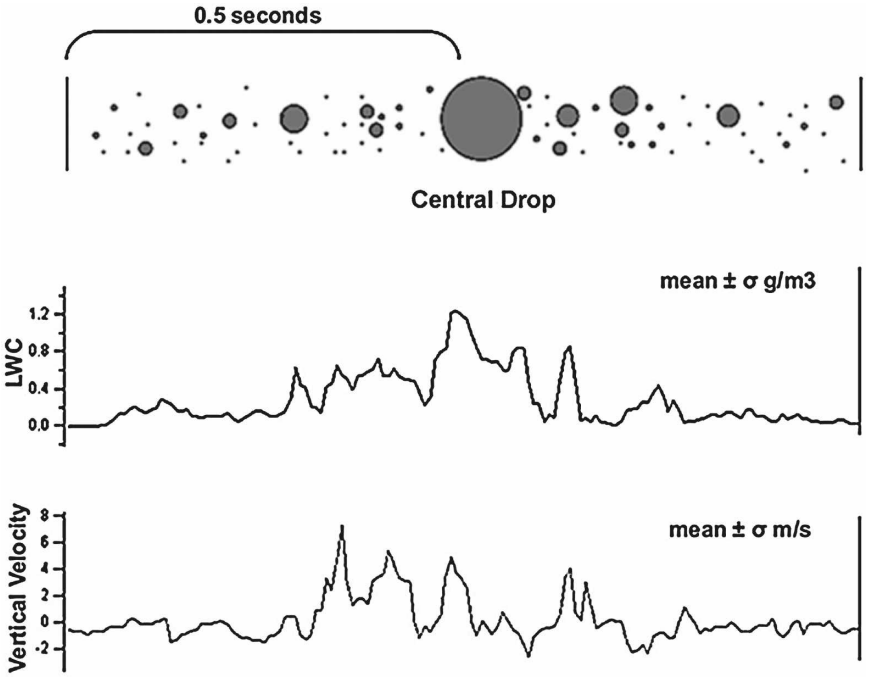

FIG. 4. Drop environment schematic. For every observed drop (i.e., the central drop), we select an environment beginning 0.5 s prior to the drop arrival and ending 0.5 s after, for a total time envelope of 1 s. The mean and standard deviation of a number of parameters (LWC and w shown here) within this envelope, all measured at 25 Hz, are calculated. In addition, the cloud drop size distribution is also determined from PDI measurements.

drops remaining after filtering, ~3% are considered CCIs with $D_p > 55$ μm. Figure 6 shows observed N_{CCI}/N_d, N_d, LWC, and w in the 1-s environments. Figure 7 shows observed θ, θ_e, and θ_v (see Fig. 5 caption for axis explanation and notation). To simplify the analysis, we will compare and contrast the environments surrounding central drops of three different size ranges: small ($D_p < 15$ μm), intermediate (25 μm $< D_p <$ 40 μm), and CCI ($D_p > 55$ μm). Table 1 summarizes the environmental characteristics for these different size classes.

If we first examine envelopes surrounding drops in the intermediate size range (25 μm $< D_p <$ 40 μm), which constitute the bulk of drops remaining after filtering at the altitude of interest, we observe that size distribution shape in the surrounding environment remains fairly constant with mean values of D_{10}, D_{50}, and D_{90} of 21 $\pm$ 5, 28 $\pm$ 5, and 36 $\pm$ 9 μm respectively (uncertainties are 1σ of observed variability). In Fig. 6 we see that the general pattern is that of constant N_{CCI}/N_d, fairly constant LWC and N_d, and w close to zero but slightly positive. Note that the combination of constant D_{10}, D_{50}, and D_{90} and constant N_d implies a reasonably constant cloud drop size distribution. In Fig. 7 we see that the general trend for intermediate drops is that of fairly constant θ, θ_e, and θ_v, with minimum values of θ observed in this size range. This suggests that intermediate drops are on average present in similar environments and thus have similar average histories. Had drops experienced grossly different trajectories and entrainment events throughout their history, differences in drop growth rates and thus the size distribution shape, as well as differences in thermodynamic quantities in their surrounding environments, would be expected among the 1-s environments. Detailed analyses of drop trajectories by Lasher-Trapp et al. (2005) using a single cloud model coupled to a Lagrangian microphysical parcel model illustrate such events. In contrast, central drops much smaller or larger than those in the intermediate range exhibit environments that are on average very different, indicating a systematic difference in the processes that led to their production, as will be discussed next.

For small drop ($D_p < 15$ μm) environments, we observe that mean values of D_{10}, D_{50}, and D_{90} shift to smaller sizes as compared to intermediate drops with values of 12 $\pm$ 4, 19 $\pm$ 6, and 29 $\pm$ 13 μm, respectively, representing decreases of 43%, 32%, and 19% compared to intermediate drop environments. This means that on average, a small drop is surrounded by smaller

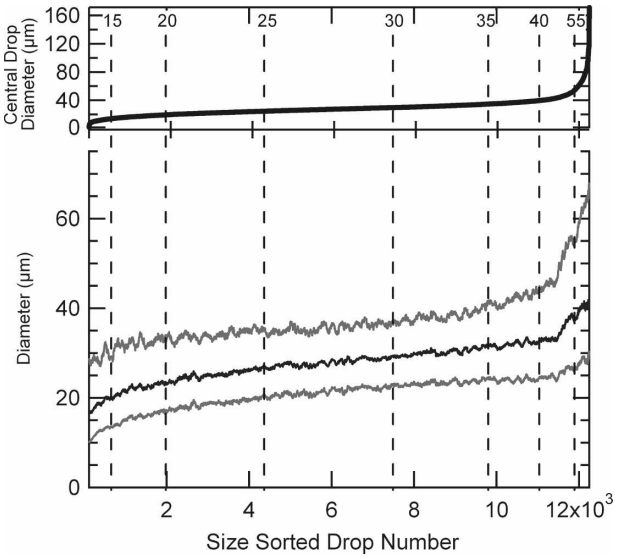

FIG. 5. Cloud drop size distribution in the environments surrounding observed drops, sorted by size (see text for explanation and Fig. 4 for schematic). Upper curve shows the size of the central drop, with the results sorted by size increasing from left to right, with 15, 20, 25, 30, 35, 40, and 55 μm demarcated by dotted lines for reference. Only drops from cloud tops of shallow cumulus (CT in Fig. 3) are included in this analysis. Lower curves show the shape of the drop size distribution in the 1-s envelope surrounding each drop plotted as D_{10} (light gray), D_{50} (dark gray), and D_{90} (light gray). There are ~350 observed CCIs, which were distributed over ~175 1-Hz samples.

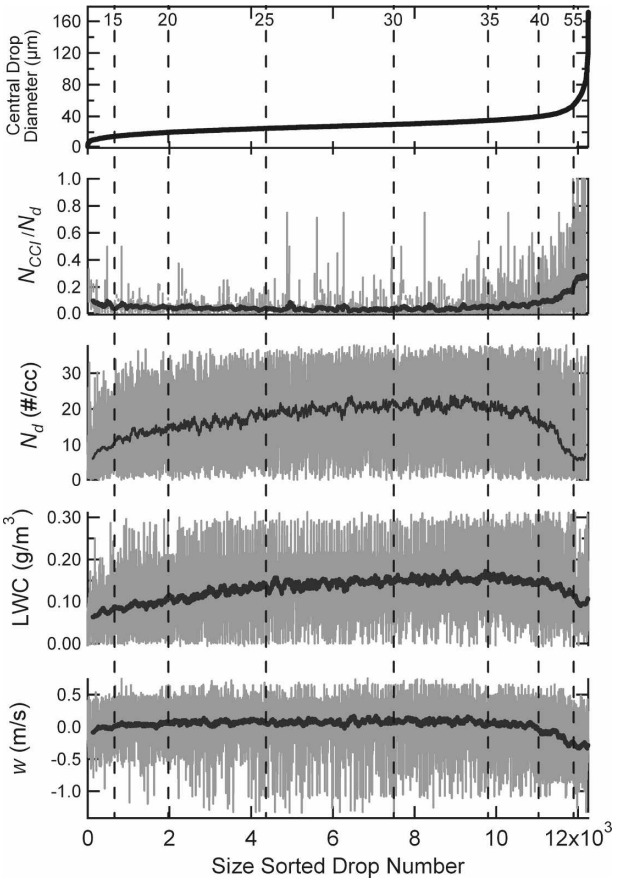

FIG. 6. Environment characteristics for all observed drops, sorted by size, reported as 1-s envelope means of N_{CCI}/N_d, N_d, LWC, and w. See Fig. 5 for description of upper curve. Light gray curves represent individual environmental means and dark gray curves show a 120-drop running mean. Mean and standard deviations for N_{CCI}/N_d, N_d, LWC, and w for $D_p < 15$ μm, 25 μm $< D_p < 40$ μm, and $D_p > 55$ μm are calculated and shown in Table 1.

drops as compared to an intermediate drop. This small drop size range exhibits the lowest mean LWC and N_d as compared to all other sizes; w is also slightly lower than for intermediate drops. We attribute the statistically significant ($p < 0.01$) decreases in LWC to cloud parcels that have experienced maximum entrainment of unsaturated air. Lower values of N_d are indicative of inhomogeneous mixing, whereas decreases in D_{10}, D_{50}, and D_{90} are characteristic of homogeneous mixing. Drops in this smallest size class are also found to have higher θ and θ_v values than intermediate drops and CCIs. These thermodynamic observations of small drop environments are also consistent with regions of greatest entrainment mixing because, in general, clear air soundings show increases of these quantities with altitude (see Fig. 2). Assuming that entrainment occurs primarily at cloud top, we would expect more diluted parcels to have higher values of θ and θ_v.

For CCI ($D_p > 55$ μm) environments, we observe a strong shift in the size distribution toward larger sizes as compared to intermediate-sized drop environments. Average observed D_{10}, D_{50}, and D_{90} values are 29 ± 15, 41 ± 16, and 63 ± 21 μm respectively, representing increases of 38%, 46%, and 75% over intermediate drop environments. Note that D_{90} values shift much more than D_{10} or D_{50}, indicating a broadening of the size distribution at larger sizes. This shift in the size distribution and the increase in N_{CCI}/N_d (see Fig. 6) surrounding CCIs demonstrate that CCIs tend to be found in the presence of other CCIs. This is supported by the distribution of CCI occurrence in 1-s envelopes; CCIs are found in clusters of five or more in only 1% of the 1-s envelopes surrounding small central drops, 7% of the 1-s envelopes surrounding intermediate-sized central drops, and 30% of the 1-s envelopes surrounding CCIs. Central drops that are CCIs have a maximum number of CCIs per envelope of 10, whereas for small drops the maximum is four per envelope.

These observations inform us about the length scales associated with the production of CCIs, given that our averaging length scale is ~100 m. The observed clouds have a typical width of ~1 km. This serves as an abso-

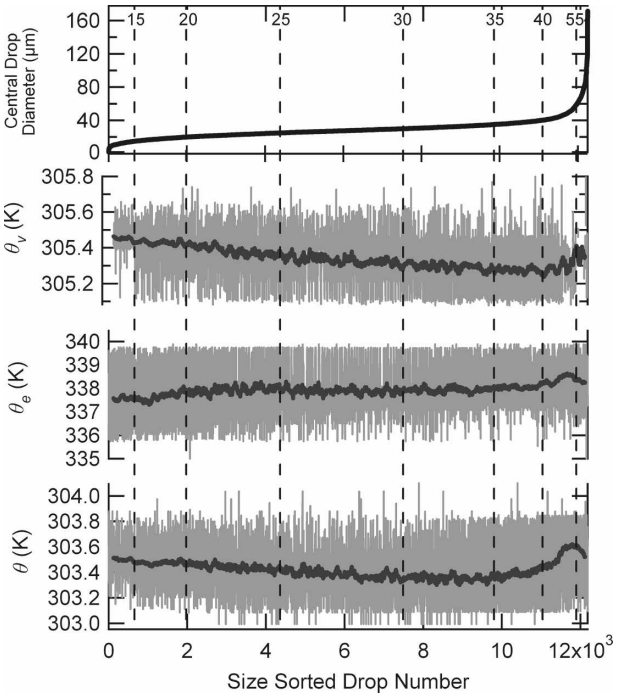

FIG. 7. As in Fig. 6, but plotting thermodynamic parameters θ, θ_e, and θ_v.

TABLE 1. Number of samples, mean, and σ for variables shown in Figs. 5–7 for small-drop ($D_p < 15$ μm), intermediate-drop (25 μm $< D_p <$40 μm), and CCI ($D_p > 55$ μm) environments. We compared the envelope means for CCIs ($D_p > 55$ μm) across all parameters shown in Figs. 5–7 with both the intermediate size range ($25 < D_p < 40$ μm) and the small size range ($D_p < 15$ μm) as well as the means between the small and intermediate ranges. Means for CCIs were always statistically different ($p < 0.01$) except when comparing the means of N_{CCI}/N_d and θ_v for small and intermediate drops.

	$D_p < 15$ μm	25 μm $< D_p <$ 40 μm	$D_p > 55$ μm
Sample size (#/envelope)	650	6600	350
D_{10} (μm)	12 ± 4	21 ± 5	29 ± 15
D_{50} (μm)	19 ± 6	28 ± 5	41 ± 16
D_{90} (μm)	29 ± 13	36 ± 9	63 ± 21
LWC (g m^{-3})	0.08 ± 0.4	0.15 ± 0.07	0.10 ± 0.06
PDI N_d (cm^{-3})	9 ± 6	20 ± 10	6 ± 7
FSSP N_d (cm^{-3})	16 ± 9	20 ± 8	14 ± 8
w (m s^{-1})	−0.02 ± 0.23	0.07 ± 0.31	−0.29 ± 0.36
θ (K)	303.5 ± 0.1	303.4 ± 0.2	303.6 ± 0.2
θ_e (K)	337.6 ± 1.0	337.9 ± 0.8	338.3 ± 0.8
θ_v (K)	305.6 ± 0.2	305.5 ± 0.2	305.7 ± 0.2

lute upper limit on the production length scale of CCIs (assuming we are sampling CCIs in the region where they formed or at least very close to it) because the vertical velocities observed at this level are very low, limiting the movement of air parcels at the time of sampling. However, the fact that many 1-s envelopes, primarily the ones surrounding small and intermediate drops, contain very few CCIs implies that not all places at cloud top are good source regions of CCIs. Thus, the upper limit for the length scale of CCI production regions is probably closer to 100 m than 1 km. This is consistent with the idea that tops of cumuli tend to exhibit characteristic circulation patterns (Blyth 1993), which we hypothesize leads to specific regions at cloud top that are favorable for CCI production. It is possible that a small fraction of CCIs can be transported up from lower levels, but production either at cloud top or somewhere between midcloud and cloud top must dominate because of the much larger fraction of CCIs observed at cloud top (Fig. 3b). Note that radar observations of warm clouds typically show initiation of precipitation occurring near cloud top, suggesting that CCIs tend to be produced in the vicinity of cloud top.

Our results also constrain the minimum length scale for CCI production regions. There are two scenarios in which the results from Figs. 5 and 6 could be obtained. In scenario A, the production of CCIs occurs in very small regions (say 5 m), but these regions have a typical spacing of ~100 m; in scenario B, the production of CCIs occurs throughout regions with a typical length scale of ~100 m. Analysis of the interdrop spacing resolves these two possibilities, and shows that the spacing is well described by an exponential distribution, with a *e*-folding length scale of ~40 m. Therefore, there is no preferential clustering at very small length scales, which eliminates scenario A and leaves scenario B as the only plausible one. Our analysis constrains the length scale in scenario B to be an appreciable fraction of 100 m because if it were much smaller, say 10 m, then the other 90 m would have characteristics more similar to that of the majority of envelopes (i.e., those of the intermediate drops) and therefore the strong shifts in all the environmental parameters plotted in Figs. 5 to 7 would not be observed. We conclude, therefore, that CCIs are found, and most likely produced, in regions that are not too different (either much larger or much smaller) from that of the length scale of our analysis, ~100 m.

The statistically significant decrease ($p < 0.01$) in LWC for CCI envelopes, as compared to those for intermediate drops, corresponds with decreases in N_d, which is consistent with inhomogeneous mixing; increases in D_{10}, D_{50}, and D_{90}, however, indicate that some growth process, either condensation or collision–coalescence (or both), was also active at some point in the envelope's history. (We will examine these pro-

cesses in the next section using a simple mixing and condensation model). In contrast, the small drop envelopes showed evidence of homogeneous mixing through the shift of drop size distributions to smaller sizes as compared to intermediate drop envelopes. Negative w for CCI envelopes (as compared to ~0 for small and intermediate envelopes) in conjunction with low LWC suggests that CCIs are preferentially found in downdrafts, likely the result of evaporative cooling caused by strong entrainment mixing. Increases in θ and θ_v (Fig. 7) for CCI environments are also consistent with increased influence of entrainment as explained above. We examined whether CCIs are found preferentially at cloud edge versus cloud interiors and see no systematic preference, suggesting that the downdrafts in which CCIs are found are not exclusively associated with the large-scale downdraft circulation found at cloud edge described by Blyth (1993). Interestingly, CCIs are found in more positively buoyant environments as indicated by higher values of θ_v, leading to a picture in which CCIs are contained in falling, but decelerating, air parcels.

We also note that when looking at size-sorted drop environments rather than fixed-frequency time series of individual cloud penetrations, mean values of θ do not fluctuate in phase with droplet number as previously observed by Paluch and Knight (1984). The differences in our results can be explained by differences in meteorological conditions—Paluch and Knight (1984) examined vigorous continental Colorado cumulus in low-humidity conditions whereas we examined maritime cumulus in humid conditions—and by the fact that the PDI observed drop size range, reaching drop sizes ~200 μm, surpasses that of the observations used in this earlier work, which considered drops only as large as 30 μm. In this case, entrainment led to a decrease in θ, which is opposite to the case described here.

We also observe that CCIs are found in highly variable environments, with LWC, N_d, and w having the highest relative variability as compared to intermediate and small drop environments. The variability of the different size ranges is calculated using the full number of samples in each size range (~650 for $D_p < 15$ μm, ~6600 for 25 μm $< D_p <$ 40 μm and ~350 for $D_p > 55$ μm). We attribute this increased variability to increased turbulence in the CCI environments resulting from the increased evaporative cooling and entrainment mixing in these regions. To insure that the higher variability of CCI envelopes is not a result of sample size, the variability of subsamples, equal to the number of CCI envelopes, from the beginning, middle, and end of the small and intermediate size ranges was calculated. We see that variability in the small and intermediate drops remains essentially the same, lower than that for CCI envelopes, regardless of the size of the sample. Lastly, we note that although small drops and CCIs exhibit similar environmental LWC (0.08 $\pm$ 0.04 and 0.10 $\pm$ 0.06 g m^{-3}), the large differences in drop size distributions show that they are, on average, present in completely distinct parts of the cloud at this sampling altitude.

5. Mixing and condensation model

Studies have investigated the process of entrainment mixing and the potential effects on cloud drop spectra (Baker and Latham 1979; Baker et al. 1980; Telford et al. 1984; Politovich 1993; Blyth 1993; Brenguier and Chaumat 2001; Lasher-Trapp et al. 2005) and have described how inhomogeneous entrainment mixing can decrease drop concentrations in an air parcel. If this parcel is subsequently lifted, additional liquid water will condense onto the remaining drops to produce a smaller number of larger drops compared to the no-entrainment case. Here we utilize a simple model of this process (Fig. 8) to examine if it can produce cloud drop size distributions characteristic of observed CCI environments. This model is similar to, though more simple than, the β^2 scheme of Brenguier and Chaumat (2001). The model is initialized with an average adiabatic cloud drop size distribution near the cloud base developed from aircraft observations at that level. The parcel is then raised adiabatically to some height, at which inhomogeneous entrainment decreases LWC by some prescribed amount that decreases N_d. The parcel is then adiabatically raised to cloud-top height and the resulting modeled size distribution is compared to observations. (See Fig. 8 for more details.) When unsaturated air mixes inhomogeneously, N_d decreases, which causes the liquid water to condense on fewer drops when the air is subsequently raised to cloud top, thus shifting the size distribution to larger sizes relative to a perfectly adiabatic parcel model.

Figure 9 shows model results. As expected, the entrainment plus condensation simulations predict an increase in D_{50} as the ratio of entrained air to cloudy air is increased for all modeled entrainment levels, with the most pronounced changes in D_{50} occurring when air is entrained close to cloud base, as expected. Figure 9 shows that this model predicts D_{10} and D_{50} values larger than those observed in the environments surrounding CCIs. In contrast, D_{90} values predicted by the model are smaller than those observed in almost all cases. As a result, the model-predicted distributions are not as broad as the observations at either the small (D_{10}) or large (D_{90}) sizes. The widths of the modeled

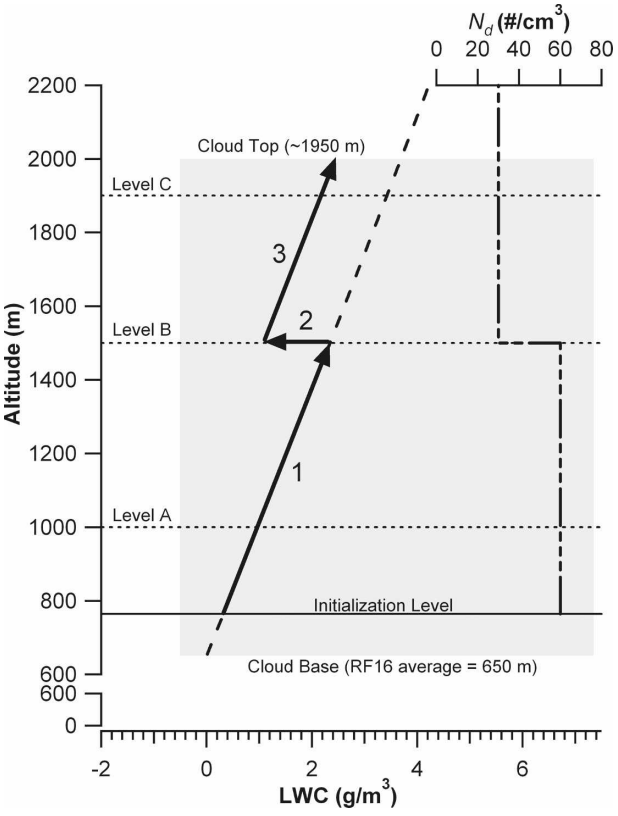

FIG. 8. Entrainment and condensation mixing model schematic. The cloudy region is represented by the gray shaded area in which all of the calculations are made. The adiabatic LWC (dotted line) increases with height above cloud base. The model is initialized ~100 m above cloud base with an average adiabatic size distribution based on observations at that level. Step 1 raises the parcel adiabatically to one of 3 levels (A to C). Level B is illustrated here. During this step, liquid water is condensed on drops as a function of the drop surface area, shifting the drop size distribution toward larger sizes. Step 2 entrains air inhomogeneously at level B, decreasing LWC and N_d (triple dashed line) by some prescribed amount (a 50% decrease in LWC and N_d is illustrated here). For step 3, the parcel is adiabatically raised to cloud top (~1950 m), again condensing liquid water as a function of drop surface area and shifting the drop size distribution. The resulting modeled distribution is then compared to observed size distributions (see Fig. 9).

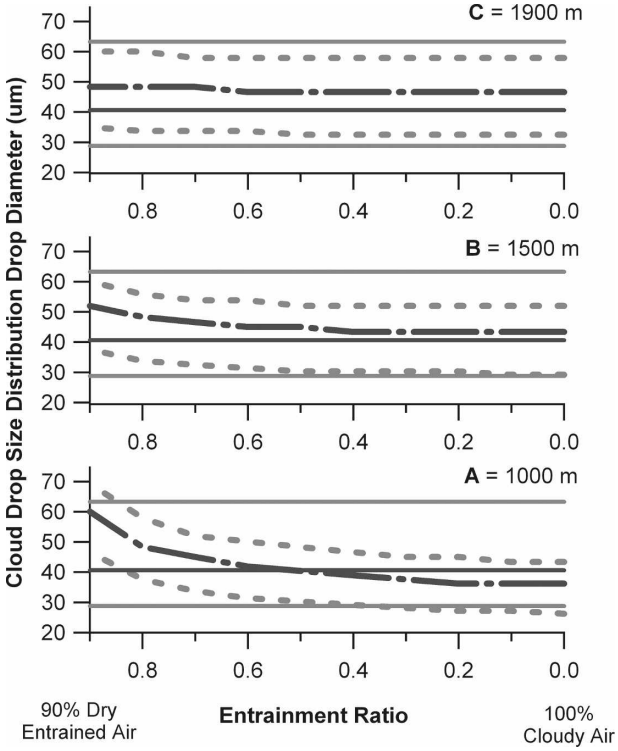

FIG. 9. Comparison of mixing and condensation model with observations. Drop diameters at D_{10}, D_{50}, and D_{90} (thick light gray, dark gray, and light gray) for modeled and observed drop size distributions at cloud top. The lowermost panel shows the modeled cloud top distributions (dotted lines) for all ratios when dry air was entrained close to cloud base (A), the central panel shows model results for the midcloud entrainment level (B) and the upper panel shows results for close to cloud top (C). The mean observed D_{10}, D_{50}, and D_{90} for CCIs are shown as solid lines. As greater amounts of entrainment shift modeled drop concentrations to smaller values, allowing liquid water to condense onto fewer drops, larger cloud top sizes are observed.

drop size distribution at cloud top, as measured by the difference between D_{90} and D_{10}, are 18, 22, and 25 μm (for air entrained at levels A, B, and C, respectively) as compared with 35 $\pm$ 19 μm for the observed drops. For each entrainment level, the modeled distributions maintain a similar symmetrical spectral width regardless of the amount of entrainment, in contrast to the asymmetrical observed distributions. Also, we note that the cases that generate the largest modeled drop sizes are also ones where the LWC would also be very close to adiabatic because entrainment occurs at the lowest altitudes of the cloud. This is inconsistent with the observed large decrease in LWC in CCI environments compared with intermediate drop environments. We conclude that the model does not match well with the observations, and, therefore, that the mechanism of inhomogeneous mixing plus condensation is insufficient to produce CCIs.

We have also run a stochastic collection model (Bott 1998) that neglects turbulence, initializing the model using an average observed drop size distribution characteristic of our intermediate size range. The results show that the production of CCIs requires 1–2 h and therefore is also insufficient to explain the observations. Recent studies suggest that collision–coalescence can be accelerated by a factor of ~2 through the inclusion of turbulence effects (Wang et al. 2006), which might better match observations.

6. Conclusions

We have analyzed observations of CCIs ($D_p > 55$ μm) measured with a PDI in shallow cumulus clouds during RICO and have investigated mechanisms for CCI production and precipitation initiation. The following is a summary of the main findings regarding CCIs.

- We find that CCIs are located predominately in cloud-top regions. Within these regions, we observe that CCIs tend to cluster together. This implies that there are regions that favor CCI production, and these regions have a length scale not very different from ~100 m.
- Our analysis shows systematic differences among the environments surrounding small ($D_p < 15$ μm), intermediate (25 μm $< D_p <$ 40 μm), and CCI ($D_p >$ 55 μm) drops.
- CCIs are found in regions that have a cloud drop size distribution strongly shifted to larger sizes, especially as measured by D_{90}.
- CCIs are found in regions that have experienced strong entrainment relative to regions surrounding intermediate drops, as evidenced by cloud microphysical (N_d, LWC) and thermodynamic (θ, θ_v) observations.
- Small drops are also found in regions that have experienced strong entrainment, but these are distinct from CCI environments, as evidenced by a shift of the local cloud drop size distribution to much smaller sizes.
- Higher variability of w, LWC, and N_d for CCI and small drop environments suggest greater turbulence in these regions, which we attribute to entrainment via negative buoyancy production from evaporative cooling.
- CCIs are found preferentially in downdrafts, in contrast to smaller drops with mean vertical velocities near zero, although we find no evidence for preference of cloud edge versus interiors.
- A simple inhomogeneous mixing and condensation model for formation of CCIs does a poor job of explaining these observations. A stochastic collection model is similarly inadequate.

Our results show that cloud-top entrainment appears to be an important ingredient in CCI formation. This is supported by previous work (Blyth 1993; Paluch 1979; Jensen et al. 1985) that stresses the importance of cloud-top processes, including entrainment and collision–coalescence, in the initiation of precipitation. We hypothesize that turbulence generated by entrainment, locally increasing the rate of collision coalescence, may play an important role, and we hope to address this in future work.

Acknowledgments. This work was supported by the National Science Foundation Programs for Physical Meteorology and Major Research Instrumentation. We acknowledge UCSC STEPS for student travel support. We thank all the NCAR RAF and UCAR JOSS personnel for their excellent technical and logistical support during the field program. We owe tremendous gratitude to Artium Technologies, in particular Will Bachalo, Khalid Ibrahim, Mike Fidrich, and Greg Payne, for their dedicated efforts, without which this work would not have been possible. We thank the RICO organizers (R. Rauber, B. Stevens, H. Ochs III, and C. Knight) for their efforts in coordinating a successful project. We also thank Sonia Lasher-Trapp and Raymond Shaw for helpful discussions.

REFERENCES

Bachalo, W., and S. V. Sankar, 1998: Phase Doppler particle analyzer. *The Handbook of Fluid Dynamics,* R. W. Johnson, Ed., CRC Press, 37-1–37-19.

Baker, M. B., and J. Latham, 1979: The evolution of droplet spectra and rate of production of embryonic raindrops in small cumulus cloud. *J. Atmos. Sci.,* **36,** 1612–1615.

——, R. G. Corbin, and J. Latham, 1980: The influence of entrainment on the evolution of cloud droplet spectra: I. A model of inhomogeneous mixing. *Quart. J. Roy. Meteor. Soc.,* **106,** 581–598.

Baumgardner, D., and M. Spowart, 1990: Evaluation of the Forward Scattering Spectrometer Probe. Part III: Time response and laser inhomogeneity limitations. *J. Atmos. Oceanic Technol.,* **7,** 666–672.

Beard, K. V., and H. T. Ochs III, 1993: Warm-rain initiation: An overview of microphysical mechanisms. *J. Appl. Meteor.,* **32,** 608–625.

Blyth, A. M., 1993: Entrainment in cumulus clouds. *J. Appl. Meteor.,* **32,** 626–641.

——, S. G. Lasher-Trapp, W. A. Cooper, C. A. Knight, and J. Latham, 2003: The role of giant and ultragiant nuclei in the formation of early radar echoes in warm cumulus clouds. *J. Atmos. Sci.,* **60,** 2557–2572.

Bott, A., 1998: A flux method for the numerical solution of the stochastic collection equation. *J. Atmos. Sci.,* **55,** 2284–2293.

Brenguier, J.-L., and L. Chaumat, 2001: Droplet spectra broadening in cumulus clouds. Part I: Broadening in adiabatic cores. *J. Atmos. Sci.,* **58,** 628–641.

Chuang, P. Y., J. D. Small, E. W. Saw, R. A. Shaw, C. M. Sipperley, G. A. Payne, and W. D. Bachalo, 2008: Airborne phase Doppler interferometry for cloud microphysical measurements. *Aerosol Sci. Technol.,* in press.

Cooper, W. A., 1988: Effects of coincidence on measurements with a Forward Scattering Spectrometer Probe. *J. Atmos. Oceanic Technol.,* **5,** 823–832.

Glantz, P., K. J. Noone, and S. R. Osborne, 2003: Comparisons of airborne CVI and FSSP measurements of cloud droplet number concentrations in marine stratocumulus clouds. *J. Atmos. Oceanic Technol.,* **20,** 133–142.

Illingworth, A. J., 1988: The formation of rain in convective clouds. *Nature,* **336,** 754–756.

Jensen, J. B., P. H. Austin, M. B. Baker, and A. M. Blyth, 1985: Turbulent mixing, spectral evolution, and dynamics in a warm cumulus cloud. *J. Atmos. Sci.,* **42,** 173–192.

Johnson, D. B., 1976: Ultragiant urban aerosol particles. *Science,* **194,** 941–942.

——, 1982: The role of giant and ultragiant aerosol particles in warm rain initiation. *J. Atmos. Sci.,* **39,** 448–460.

——, 1993: The onset of effective coalescence growth in convective clouds. *Quart. J. Roy. Meteor. Soc.,* **119,** 925–933.

Jonas, P. R., 1996: Turbulence and cloud microphysics. *Atmos. Res.,* **40,** 283–306.

Khain, A. P., and M. B. Pinsky, 1997: Turbulence effects on the collision kernel. II: Increase of the swept volume of colliding drops. *Quart. J. Roy. Meteor. Soc.,* **123,** 1543–1560.

Laird, N. F., H. T. Ochs III, R. M. Rauber, and L. J. Miller, 2000: Initial precipitation formation in warm Florida cumulus. *J. Atmos. Sci.,* **57,** 3740–3751.

Lasher-Trapp, S. G., C. A. Knight, and J. M. Straka, 2001: Early radar echoes from ultragiant aerosol in a cumulus congestus: Modeling and observations. *J. Atmos. Sci.,* **58,** 3545–3562.

——, W. A. Cooper, and A. M. Blyth, 2002: Measurements of ultragiant aerosol particles in the atmosphere from the Small Cumulus Microphysics Study. *J. Atmos. Oceanic Technol.,* **19,** 402–408.

——, ——, and ——, 2005: Broadening of droplet size distributions from entrainment and mixing in a cumulus cloud. *Quart. J. Roy. Meteor. Soc.,* **131,** 195–220.

Latham, J., and R. L. Reed, 1977: Laboratory studies of the effects of mixing on the evolution of cloud droplet spectra. *Quart. J. Roy. Meteor. Soc.,* **103,** 297–306.

Meszaros, A., and K. Vissy, 1974: Concentration, size distribution and chemical nature of atmospheric aerosol particles in remote oceanic areas. *J. Aerosol Sci.,* **5,** 101–109.

Noll, K. E., and M. J. Pilat, 1971: Size distribution of atmospheric giant particles. *Atmos. Environ.,* **5,** 527–540.

Paluch, I. R., 1979: The entrainment mechanism in Colorado cumuli. *J. Atmos. Sci.,* **36,** 2467–2478.

——, and C. A. Knight, 1984: Mixing and the evolution of cloud droplet size spectra in a vigorous continental cumulus. *J. Atmos. Sci.,* **41,** 1801–1815.

Pinsky, M. B., and A. P. Khain, 1996: Simulations of drop fall in a homogeneous isotropic turbulence flow. *Atmos. Res.,* **40,** 223–259.

——, ——, and M. Shapiro, 1999: Collisions of small drops in a turbulent flow. Part I: Collision efficiency. Problem formulation and preliminary results. *J. Atmos. Sci.,* **56,** 2585–2600.

Politovich, M. K., 1993: A study of the broadening of droplet size distributions in cumuli. *J. Atmos. Sci.,* **50,** 2230–2244.

Rauber, R. M., and Coauthors, 2007: Rain in shallow cumulus over the ocean: The RICO campaign. *Bull. Amer. Meteor. Soc.,* **88,** 1912–1928.

Rogers, R. R., and M. K. Yau, 1989: *A Short Course in Cloud Physics*. 3rd ed. Pergamon Press, 292 pp.

Sankar, S. V., K. M. Ibrahim, D. H. Buermann, A. S. Inenaga, and W. D. Bachalo, 1994: Coherent scattering in phase Doppler interferometry: Response of frequency domain processors. *Proc. Seventh Int. Symp. on the Application of Laser Techniques to Fluid Mechanics,* Lisbon, Portugal, European Office of Aerospace Research and Development.

Shaw, R. A., 2003: Particle–turbulence interactions in atmospheric clouds. *Ann. Rev. Fluid Mech.,* **35,** 183–227.

——, W. C. Reade, L. R. Collins, and J. Verlinde, 1998: Preferential concentration of cloud droplets by turbulence: Effects on the early evolution of cumulus cloud droplet spectra. *J. Atmos. Sci.,* **55,** 1965–1976.

Squires, P., 1958: The spatial variation of liquid water and droplet concentration in cumuli. *Tellus,* **10,** 372–380.

Strakey, P. A., D. G. Talley, S. V. Sankar, and W. D. Bachalo, 2000: Phase-Doppler interferometry with probe-to-droplet size ratios less than unity. II. Application of the technique. *Appl. Opt.,* **39,** 3887–3893.

Telford, J. W., T. S. Keck, and S. K. Chai, 1984: Entrainment at cloud tops and the droplet spectra. *J. Atmos. Sci.,* **41,** 3170–3179.

Tisler, P., E. Zapadinsky, and M. Kulmala, 2005: Initiation of rain by turbulence-induced condensational growth of cloud droplets. *Geophys. Res. Lett.,* **32,** L06806, doi:10.1029/2004GL021969.

Vaillancourt, P. A., and M. K. Yau, 2000: Review of particle–turbulence interactions and consequences for cloud physics. *Bull. Amer. Meteor. Soc.,* **81,** 285–298.

Vohl, O., S. K. Mitra, S. C. Wurzler, and H. R. Pruppacher, 1999: A wind tunnel study of the effects of turbulence on the growth of cloud drops by collision and coalescence. *J. Atmos. Sci.,* **56,** 4088–4099.

Wang, L.-P., Y. Xue, O. Ayala, and W. W. Grabowski, 2006: Effects of stochastic coalescence and air turbulence on the size distribution of cloud droplets. *Atmos. Res.,* **82,** 416–432.

Warner, J., 1969a: The microstructure of cumulus cloud. Part I. General features of the droplet spectrum. *J. Atmos. Sci.,* **26,** 1049–1059.

——, 1969b: The microstructure of cumulus cloud. Part II: The effect on droplet size distribution of the cloud nucleus spectrum and updraft velocity. *J. Atmos. Sci.,* **26,** 1272–1282.

——, 1970: On steady-state one-dimensional models of cumulus convection. *J. Atmos. Sci.,* **27,** 1035–1040.

——, 1973: The microstructure of cumulus cloud. Part IV: The effect on the droplet spectrum of mixing between cloud and environment. *J. Atmos. Sci.,* **30,** 256–261.

Widmann, J. F., C. Presser, and S. D. Leigh, 2001: Improving phase Doppler volume flux measurements in low data rate applications. *Meas. Sci. Technol.,* **12,** 1180–1190.